The E3 ubiquitin ligase UBR5 regulates centriolar satellite stability and primary cilia

Robert F. Shearer[a,b], Kari-Anne Myrum Frikstad[c], Jessie McKenna[d], Rachael A. McCloy[a], Niantao Deng[a], Andrew Burgess[a,b], Trond Stokke[c], Sebastian Patzke[c], and Darren N. Saunders[d,*]

[a]Garvan Institute of Medical Research, Kinghorn Cancer Centre, Darlinghurst 2010, Australia; [b]Faculty of Medicine, St. Vincent's Clinical School, and [d]Faculty of Medicine, School of Medical Sciences, University of New South Wales, Sydney 2052, Australia; [c]Department of Radiation Biology, Institute for Cancer Research, Norwegian Radium Hospital, Oslo University Hospital, 0310 Oslo, Norway

ABSTRACT **Primary cilia are crucial for signal transduction in a variety of pathways, including hedgehog and Wnt. Disruption of primary cilia formation (ciliogenesis) is linked to numerous developmental disorders (known as ciliopathies) and diseases, including cancer. The ubiquitin–proteasome system (UPS) component UBR5 was previously identified as a putative positive regulator of ciliogenesis in a functional genomics screen. UBR5 is an E3 ubiquitin ligase that is frequently deregulated in tumors, but its biological role in cancer is largely uncharacterized, partly due to a lack of understanding of interacting proteins and pathways. We validated the effect of *UBR5* depletion on primary cilia formation using a robust model of ciliogenesis, and identified CSPP1, a centrosomal and ciliary protein required for cilia formation, as a UBR5-interacting protein. We show that UBR5 ubiquitylates CSPP1, and that UBR5 is required for cytoplasmic organization of CSPP1-comprising centriolar satellites in centrosomal periphery, suggesting that UBR5-mediated ubiquitylation of CSPP1 or associated centriolar satellite constituents is one underlying requirement for cilia expression. Hence, we have established a key role for UBR5 in ciliogenesis that may have important implications in understanding cancer pathophysiology.**

Monitoring Editor
Yixian Zheng
Carnegie Institution

Received: Apr 18, 2017
Revised: Apr 23, 2018
Accepted: Apr 30, 2018

INTRODUCTION

Primary cilia form at the surface of most mammalian cell types, and have been implicated in sensory perception, cell signaling, and development. Primary cilia comprise a microtubule (MT) axoneme and ciliary membrane extending from the basal body (Satir and Christensen, 2007), which is surrounded by granular structures known as centriolar satellites (Figure 1A; Lopes *et al.*, 2011) largely composed of pericentriolar material 1 (PCM1) and other key proteins (Kubo *et al.*, 1999). In contrast to motile cilia, primary cilia lack the core MT/dynein structure that provides motility to the former (Roth *et al.*, 1988). During mammalian development, primary cilia

This article was published online ahead of print in MBoC in Press (http://www.molbiolcell.org/cgi/doi/10.1091/mbc.E17-04-0248) on May 9, 2018.

*Address correspondence to: Darren N. Saunders (d.saunders@unsw.edu.au).

Abbreviations used: ATMIN, ATM interactor; ATP, adenosine triphosphate; BiFC, bimolecular fluorescence complementation; CCLE, Cancer Cell Line Encyclopaedia; Ci, cubitus interruptus; CSPP, spindle pole associated protein; CSPP-L, spindle pole associated protein large; CSPP1, centrosome and spindle pole associated protein 1; DOX, doxycycline; Dpp, decapentaplegic; E3, E3 ubiquitin ligase; E6.0, embryonic day 6.0; EDD, E3 ligase identified by differential display; ExAC, Exome Aggregation Consortium; GFP, green fluorescent protein; GLI1, GLI family zinc finger 1; GLI2, GLI family zinc finger 2; Glut, glutamic acid; H2B, histone H2B; H3, histone H3; HECT, homologous to E6AP at the carboxy terminus; Hh, hedgehog; HHIP, hedgehog interacting protein; Hyd, hyperplastic disks; IB, immunoblot; IP, immunoprecipitation; K29, lysine 29; K48, lysine 48; K63, lysine 63; LGMN, legumain; LoF, loss of function; MIB1, mindbomb 1; MIF, macrophage migration inhibitory factor; MLF, MLF-type n-degron; MLLE, MLLE domain; MOI, multiplicity of infection; MT, microtubule; NB, nonbound; NCI, National Cancer Institute; NFkB, nuclear factor kappa-light-chain-enhancer of activated B cells; ORF, open reading frame; OTUD6B, OTU domain containing 6B; p53, tumor protein 53; PCM1, percentriolar material 1; poly-Ub, poly-ubiquitin; PTCH1, patched 1; px, pixel; RIPA, radioimmunoprecipitation assay; RNAi, RNA interference; ROI, region of interest; RPE, retinal pigment epithelial; SEEK, search-based exploration of expression compendia; SEPT7, septin 7; shNT, short hairpin nontargeting; shRNA, short hairpin RNA; shUBR5, short hairpin to UBR5; siGFP, short interfering RNA to GFP; siPCM1, short interfering RNA to PCM1; siRNA, short interfering RNA; siUBR5, short interfering RNA to UBR5; SMAD4, SMAD family member 4; SUMF1, sulfatase modifying factor 1; TCGA, The Cancer Genome Atlas; TERT, telomerase reverse transcriptase; Ub, ubiquitin; UBR, UBR box; UBR5, ubiquitin protein ligase E3 component n-recognin 5; UPS, ubiquitin proteasome system; V1, Venus fragment 1; V2, Venus fragment 2; WCE, whole cell extract; WDHD1, WD repeat and HMG-box DNA binding protein 1; YTHDF3, YTH N6-methyladenosine RNA binding protein 3.

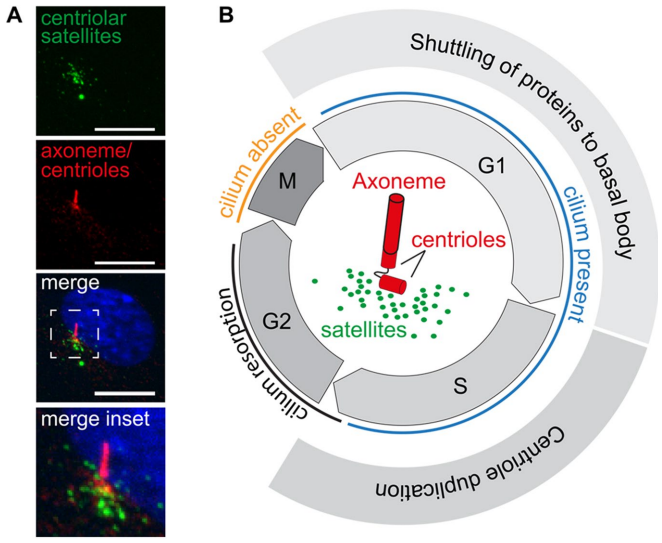

FIGURE 1: Centriolar satellites as regulators of centrosomal function. (A) Centriolar satellites localize to the pericentriolar space surrounding the centrioles. Cilium and centrioles stained with an antibody to glutamylated-tubulin (red), and satellites stained with antibody to PCM1 (green). Nuclear marker Hoechst33258 (blue). High-powered inset fields are indicated by a dashed box. Confocal imaging, bar = 10 µm. (B) Centriolar satellites are required for shuttling of centrosomal proteins to the basal body from which the ciliary axoneme extends during G1 phase (Lopes *et al.*, 2011), and act in the assembly of proteins during centriole duplication in S phase (Hori and Toda, 2017).

are present from around embryonic day E6.0 and are retained throughout gestation in a lineage dependent manner (Bangs *et al.*, 2015). Multiple signaling pathways including hedgehog (Hh) require intact cilia for effective signal transduction (May *et al.*, 2005), and as such understanding the dynamics of ciliogenesis and cilia function is highly relevant to understanding development and cancer (Michaud and Yoder, 2006). Recent characterizations of the complex ciliary proteome and interactome (Pazour *et al.*, 2005; Gupta *et al.*, 2015; Mick *et al.*, 2015; Wheway *et al.*, 2015; Boldt *et al.*, 2016) demonstrate the highly organized and dynamic structure of primary cilia.

Ubiquitylation is one of the most common protein posttranslational modifications, resulting in the attachment of one or more ubiquitin (Ub) molecules to substrate proteins via an ATP-dependent enzymatic cascade known as the ubiquitin–proteasome system (UPS; Ciehanover *et al.*, 1978; Hershko *et al.*, 1981). The various signaling outcomes of protein ubiquitylation are determined by the topology of the attached poly-Ub chains (Passmore and Barford, 2004). For example, K48 linked poly-Ub target substrates for proteasomal degradation, but alternate linkages (K63, K29, etc.) are emerging as key regulators of cell signaling via modulation of protein function, localization, and protein–protein interactions. Key proteins associated with tumor initiation (e.g., p53, NF-κB) are regulated by the proteasome, and proteasome inhibitors such as PS-341 and bortezomib (Velcade) are under trial or approved for clinical use in hematological malignancies (Orlowski *et al.*, 2002; Johnson, 2014).

The integrity of centriolar satellites is crucial for centrosome-related functions, including centriole formation and ciliogenesis (Tollenaere *et al.*, 2015). Although the biology is poorly characterized, the distribution and appearance of centriolar satellites is coregulated with cell cycle progression (Kim and Rhee, 2011), to which cilium assembly/resorption and centrosome duplication are tightly linked (Figure 1B). For example, centriolar satellites regulate shuttling of cilia-related proteins to the basal body (Lopes *et al.*, 2011), and aid in the assembly of the many centrosomal components required to duplicate the centrosome (Hori and Toda, 2017).

The UPS is emerging as a key regulator of ciliogenesis and centriolar satellite stability (Shearer and Saunders, 2016). E3 Ub ligases, which largely determine substrate specificity and are an important rate-limiting component of the UPS, can regulate expression of various proteins crucial to ciliary axoneme extension. For example, the Cullin Ub ligase Mindbomb 1 (MIB1) regulates multiple centriolar proteins, including PCM1 (Villumsen *et al.*, 2013; Cajanek *et al.*, 2015), and extension of the axoneme is initiated by UPS-mediated degradation of the ciliogenesis inhibitor trichoplein (Inoko *et al.*, 2012; Kasahara *et al.*, 2014). A genome-wide RNA interference (RNAi) screen for regulators of ciliogenesis identified a number of components of the UPS (Kim *et al.*, 2010), including the E3 Ub ligase UBR5 (ubiquitin protein ligase E3 component N-recognin 5). UBR5 is a highly conserved gene (Mansfield *et al.*, 1994; Callaghan *et al.*, 1998) required for normal embryonic development, multiple aspects of the DNA damage response, and other cellular functions (Shearer *et al.*, 2015). UBR5 is frequently deregulated in many cancer types by amplification and/or mutation (Clancy *et al.*, 2003; O'Brien *et al.*, 2008; Meissner *et al.*, 2013), but the full complement of UBR5 substrates, and hence the mechanistic role of UBR5 in cancer, remain to be defined.

We sought to further investigate the role of UBR5 in ciliogenesis in a cancer context. We show that UBR5 regulates primary ciliogenesis and identify a novel interaction between UBR5 and the centriolar satellite protein CSPP1. CSPP1 is a direct substrate of UBR5 ligase activity, and depletion of *UBR5* affects the subcellular localization of CSPP1 and CSPP1-associated centriolar satellites. Identification of UBR5 as a novel ciliary regulator has interesting implications for understanding cell signaling in development and cancer.

RESULTS

Depletion of *UBR5* confers concurrent disruption of centriolar satellites and inhibition of primary cilia formation

UBR5 was identified as a putative regulator of primary cilia formation in a functional genomics screen (Kim *et al.*, 2010) along with a number of other UPS components (Shearer and Saunders, 2016). We validated the effect of UBR5 depletion on cilia formation using a robust ciliogenesis assay (Figure 2A) and examined the functional significance of UBR5 depletion in the context of cilia/centriolar satellite stability/organization. Small interfering RNA (siRNA)-mediated depletion of UBR5 almost completely attenuated primary cilia formation in hTERT-RPE1 cells (i.e., observed in fewer than 20% of cells), as determined by labeling with an antibody against glutamylated tubulin (Figure 2, B and C). Furthermore, centriolar satellites were dispersed with UBR5 depletion (Figure 2, B and C). Centriolar satellite disruption with UBR5 depletion was similar to that observed with depletion of *PCM1* (Figure 2, B and C). PCM1 has previously been shown to recruit another E3 ligase, MIB1, to the centrosome (Wang *et al.*, 2016). Cilia were absent in 89% of hTERT-RPE1 with UBR5 depletion under serum starvation, and 94% of these cells displayed dispersed centriolar satellites (Figure 2C). Approximately 77% of control hTERT-RPE1 cells expressed a primary cilium, of which 85% had distinct centriolar satellite formation around the basal body (Figure 2C). Cilia attenuation by UBR5 depletion was not cell cycle dependent, as hTERT-RPE1 cells did not accumulate in cell cycle phases considered nonpermissive for cilia formation (Supplemental Figure S1A).

Given this effect on UBR5 depletion on centriolar satellite stability, we hypothesized that UBR5 may act to stabilize centriolar

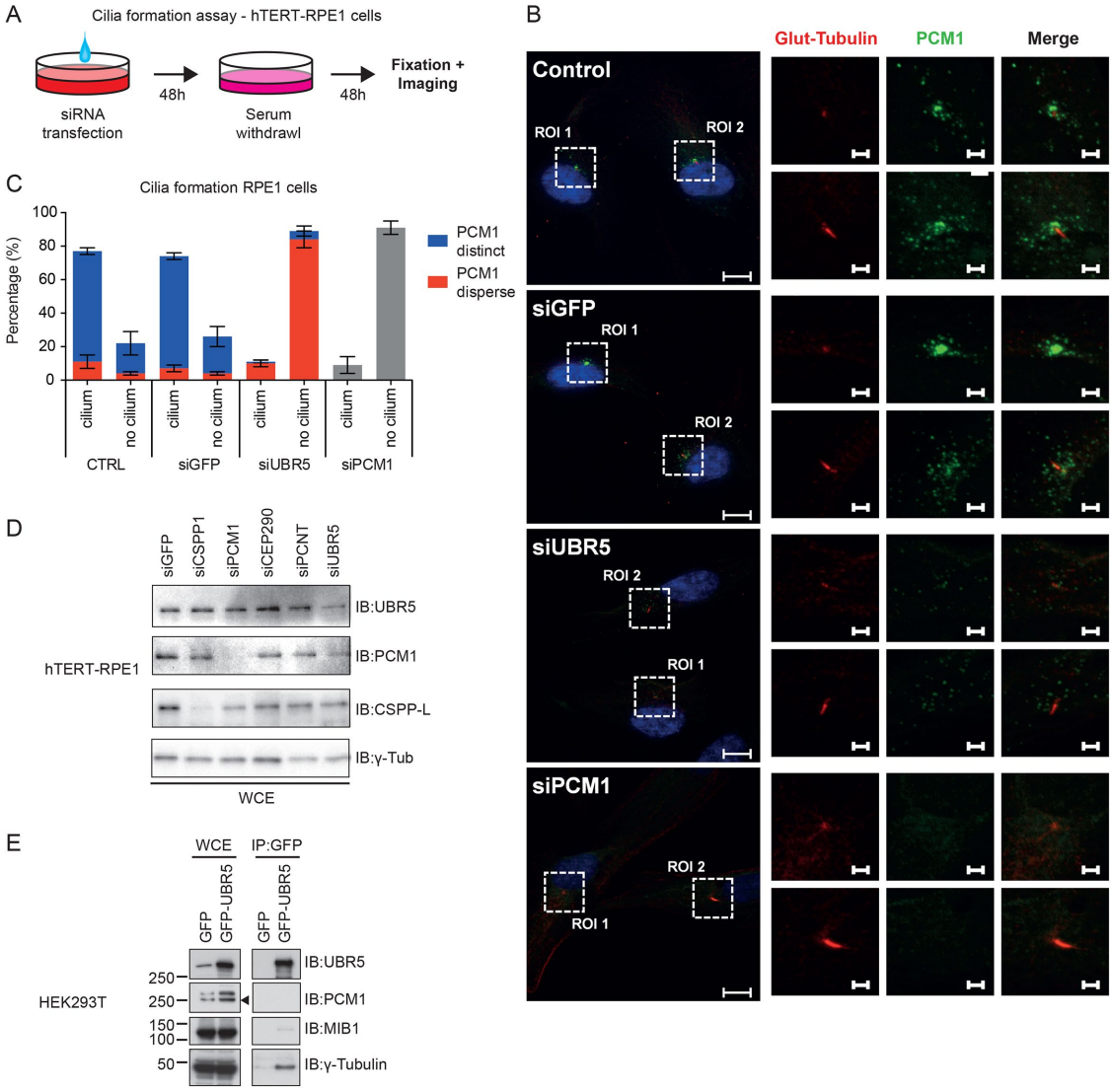

FIGURE 2: UBR5 depletion disrupts centriolar satellite stability and primary cilia formation in hTERT-RPE1 cells. (A) Schematic describing ciliogenesis assay. (B) Depletion of UBR5 attenuates primary cilia formation in and causes dispersion of centriolar satellites in RPE1 cells. Cilium and basal body stained with antibody to glutamylated tubulin (red), satellites stained with antibody to PCM1 (green), and nucleus marked with Hoechst33258 (blue). A similar phenotype is observed for depletion of PCM1. High-powered inset fields are indicated by a dashed box. Transfections performed 72 h before imaging. Data representative of two independent experiments, with 150 cells counted per condition per experiment. Confocal imaging, bar = 10 μm. High magnification of region of interest (ROI) bar = 2 μm. (C) Quantitation of data depicted in B shows the strong penetrance of siUBR5 and siPCM1 phenotype. Blue and red bars show percentage of cells with distinct or dispersed satellites, respectively. Error bars = SEM. (D) Immunoblot showing siRNA efficacy in RPE1 cells used for staining in C. (E) Coimmunoprecipitation of UBR5 and Western blotting for potential interactions with PCM1, MIB1, and γ-tubulin (a marker of the centrosome). Transfections performed 48 h before imaging. Data representative of two experiments.

material and investigated potential protein–protein interactions with known structural components of the centrosome and regulators of centriolar satellite stability. We performed pull downs of GFP-tagged UBR5 in HEK293T cells, and observed coimmunoprecipitation of UBR5 and γ-tubulin, indicating that UBR5 can interact with structural components of the centrosome (Figure 2E). The UPS is known to regulate centriolar satellite stability via MIB1-mediated ubiquitylation of PCM1 (Villumsen *et al.*, 2013; Wang *et al.*, 2016). We could not detect an interaction between UBR5 and PCM1, and we observed only a very weak putative interaction with MIB1 (Figure 2E). Furthermore, UBR5 depletion in HEK293T cells did not significantly alter levels of PCM1, MIB1, or γ-tubulin proteins (Supplemental Figure S1B). Together, these data suggest that the role of UBR5 in ciliogenesis is not mediated via directly affecting PCM1/MIB1.

Coexpression of *CSPP1* and *UBR5* in human cancer cell lines and primary cancer biopsies

To identify potential mechanisms by which UBR5 regulates cilia/centrosome biology, we analyzed publicly available gene expression datasets to identify candidate genes coregulated with *UBR5*. Coordinate expression of genes functioning in common pathways (i.e., synexpression groups) is a widespread phenomenon in eukaryotes and coexpression analysis has proven to be a powerful

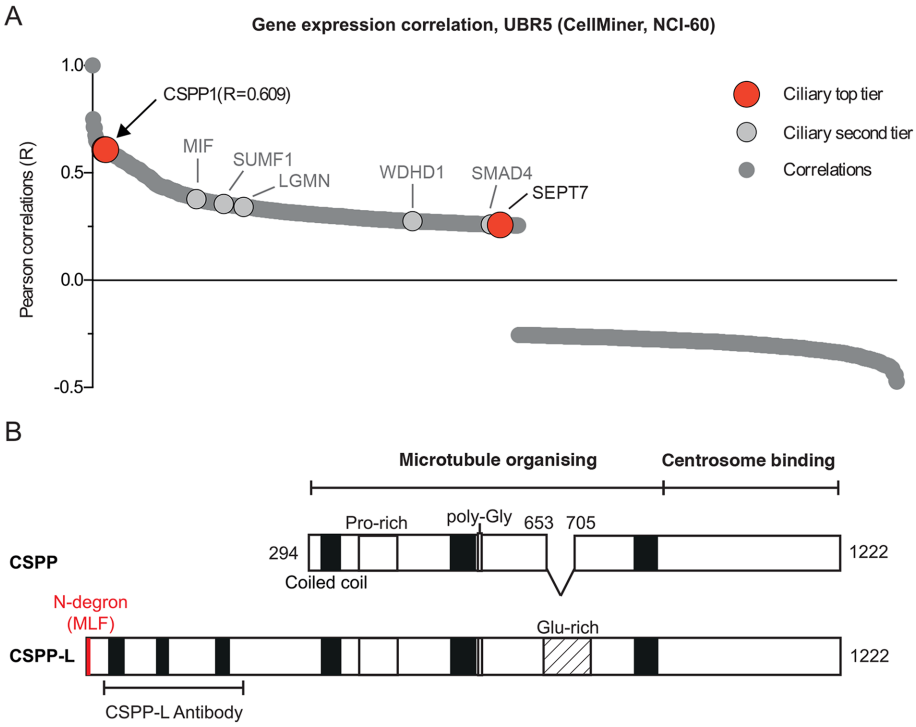

FIGURE 3: Coexpression of *UBR5* gene. (A) Waterfall plot showing global correlation of gene expression against *UBR5* expression in NCI-60 cancer cell line panel, obtained via CellMiner (Reinhold *et al.*, 2012). Cutoff set at Pearson correlation of 0.254. Putative ciliary proteins are indicated, with putative top tier cilia localizing proteins labeled and indicated with larger red dots; second tier cilia localizing proteins are also labeled and shown with larger gray dots. Putative cilia localizing proteins based on cilia proximity labeling data (Mick *et al.*, 2015). (B) Structure of CSPP1 protein isoforms. Note that the extra 294 amino acid N-terminal region of CSPP-L is the binding region of the selected CSPP1 antibody. N-Degron motif shown in red. Coiled-coil domains are shown with a black box. Proline-rich domains are shown with a white box. Glutamate-rich domains are shown with a white striped box.

approach to identify novel gene function (Eisen *et al.*, 1998; Niehrs and Pollet, 1999; Wu *et al.*, 2002; van Noort *et al.*, 2003). As *UBR5* is frequently altered in multiple cancer types (Shearer *et al.*, 2015), expression data from the NCI-60 panel of cancer cell lines were utilized (Stinson *et al.*, 1992). Analysis of mRNA coexpression in the NCI-60 panel using CellMiner (Reinhold *et al.*, 2012) revealed a strong positive correlation between *UBR5* and a number of genes (Figure 3A; Pearson correlation coefficient with $n = 60$, significance cutoff at 0.254). Many genes coexpressed with *UBR5* are in close genomic proximity on chromosome 8q22—a region of known genomic instability of solid tumors—and share common enhancer/repression elements (http://atlasgeneticsoncology.org/Indexbychrom/idxa_8.html). These genes were excluded from further consideration. Importantly, very few genes in the genomic proximity of *CSPP1* at 8q13 were coexpressed with *CSPP1*, suggesting that the observed coexpression of *UBR5* and *CSPP1* is not due simply to amplification of the entire chromosome 8q arm.

Of 855 genes significantly coexpressed with *UBR5* (Figure 3A), several have been previously identified as candidate ciliary localizing proteins (Mick *et al.*, 2015), including *centrosome and spindle pole associated protein 1* (*CSPP1*), *YTH N(6)-methyladenosine RNA-binding protein 3* (*YTHDF3*), which contains an RNA-binding YTH motif (Stoilov *et al.*, 2002), and *septin 7* (*SEPT7*), which contains a GTP-binding motif (Serrao *et al.*, 2011). The top-ranked candidate gene significantly coexpressed with *UBR5* in cancer cell lines was *CSPP1* ($p < 0.0001$). CSPP1 is enriched in primary cilia and has established functional roles in regulation of spheroid formation, cell division, and ciliogenesis (Asiedu *et al.*, 2009; Patzke *et al.*, 2010; Sternemalm *et al.*, 2015; Zhu *et al.*, 2015a). Mutations in *CSPP1* have been implicated in ciliopathies (Akizu *et al.*, 2014; Shaheen *et al.*, 2014; Tuz *et al.*, 2014), and expression of CSPP1 isoforms display distinct restriction in breast cancer subtypes (Sternemalm *et al.*, 2014). The large and predominantly expressed isoform of CSPP1, CSPP-L, localizes to the centrosome and centriolar satellites, where it is required for primary cilium formation in noncycling cells (Patzke *et al.*, 2010; Gupta *et al.*, 2015; Mick *et al.*, 2015), and dynamically relocalizes to the spindle apparatus of dividing cells, where it aids chromosome movements and cytokinesis during cell division (Patzke *et al.*, 2006; Asiedu *et al.*, 2009; Zhu *et al.*, 2015a).

Coexpression of *CSPP1* with *UBR5* in the NCI-60 cohort was confirmed by linear-regression analysis of NCI-60 cell line expression data ($R^2 = 0.3709$, $p < 0.0001$; Supplemental Figure S2A). Independent, complementary analysis of *CSPP1* expression using the SEEK database (Zhu *et al.*, 2015b) identified *UBR5* as one of the top genes coexpressed with *CSPP1* in cancer, ranked second (coexpression score 1.32, $p = 0.0001$) after OTUD6B (coexpression score 1.35, $p < 0.0001$), a deubiquitylase recently implicated in intellectual disability syndrome (Santiago-Sim *et al.*, 2017). Coexpression of *UBR5* and *CSPP1* was validated in independent breast cancer gene expression datasets from The Cancer Genome Atlas (TCGA; Supplemental Figure S2B and Supplemental Table S1), Cancer Cell Line Encyclopedia (CCLE), and METABRIC cohorts (Supplemental Table S2). Coexpression of *CSPP1* with *UBR5* was evident in all cohorts, irrespective of subtype (Supplemental Tables S1 and S2). Overexpression of *UBR5* and *CSPP1* mRNA was the predominant form of altered expression, and coamplification did not correlate with increased fraction of altered genome (Supplemental Figure S2B).

There are three known protein products of the *CSPP1* gene (Figure 3B). CSPP is a 101.5 kDa protein that contains both MT-organizing and centrosome-binding domains (Patzke *et al.*, 2005). CSPP-L contains an extra 294 amino acids at the N-terminus, and an additional 51 amino acids in the middomain, which affects how CSPP1 interacts with MTs (Patzke *et al.*, 2006). Of relevance to the ubiquitin context, the extended N-terminal region of CSPP-L harbors an N-degron motif (not present on CSPP) that likely targets CSPP-L for ubiquitylation by UBR-box E3 ubiquitin ligases (Tasaki *et al.*, 2009). A third protein isoform of *CSPP1* comprising the C-terminal 379aa of CSPP-L is highly expressed in the nucleus of luminal breast cancer cells (Sternemalm *et al.*, 2014). Western blot analysis of a panel of breast cancer cell lines showed coexpression of UBR5 and CSPP-L at the protein level ($R^2 = 0.2532$, $p = 0.017$; Supplemental Figure S2, C and D), irrespective of subtype (Supplemental Figure S2, E and F). Note that the epitope recognized by the CSPP1 antibody used in Supplemental Figure S2C is specific to the CSPP-L isoform.

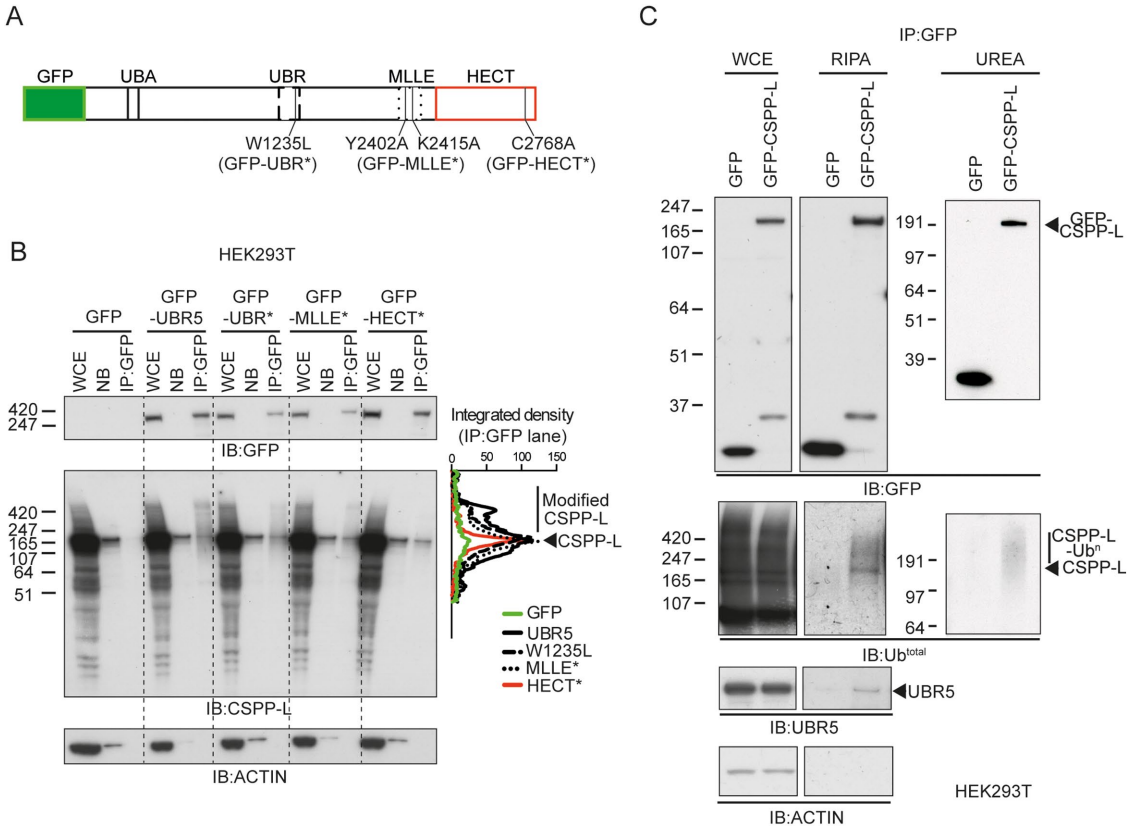

FIGURE 4: UBR5 binds and polyubiquitylates CSPP-L. (A) Schematic showing the structure of UBR5 protein and the position of known functional domains and amino acid changes of mutants. (B) Coimmunoprecipitation and immunoblot analysis of GFP-UBR5 (and functional mutants) transfected into HEK293T cells. GFP-UBR5 coimmunoprecipitates endogenous ubiquitylated CSPP-L. Covalent modification of CSPP-L is quantified by an integrated density plot showing relative size shift. Note the reduction of modified CSPP-L binding HECT* mutant. GFP-UBR5 and mutants are predicted to be approximately 338 kDa. Transfections performed 24 h before harvest. WCE, whole cell extract; NB, nonbound fraction (4% of input); IP, immunoprecipitation. Data are representative of two experiments. (C) Coimmunoprecipitation and immunoblot analysis of GFP-CSPP-L transfected into HEK293T cells. GFP-CSPP-L binds endogenous UBR5. Endogenous Ub is detected covalently bound to GFP-CSPP-L. The far right panel shows coimmunoprecipitation performed under denaturing conditions. GFP-CSPP-L is predicted to be approximately 170 kDa. Data are representative of two experiments.

UBR5 regulates ubiquitylation of CSPP-L

In the context of UBR5 and CSPP-L coexpression, common functional roles in ciliogenesis, and a recently established interaction between PCM1 and CSPP-L, and localization to centriolar satellites (Patzke *et al.*, 2012), we hypothesized that UBR5 may regulate ciliogenesis via maintenance of centriolar satellite stability/organization and possibly involving CSPP-L. We therefore investigated a possible direct interaction between UBR5 and CSPP-L in cells using a panel of GFP-tagged UBR5 variants (wild-type and functional domain mutants UBR*, MLLE*, and HECT*, as detailed in Figure 4A). Coimmunoprecipitation using GFP-UBR5 in HEK293T cells detected an interaction between UBR5 and endogenous CSPP-L, while no interaction was observed using GFP-only control (Figure 4B and Supplemental Figure S3B). Mutation of predicted functional residues in the UBR-box of UBR5 (UBR*; Matta-Camacho *et al.*, 2010), MLLE domain (MLLE*; Kozlov *et al.*, 2010; Munoz-Escobar *et al.*, 2015), or the known conserved catalytic cysteine (C2768A; Scheffner *et al.*, 1995) within the HECT active site (HECT*) had no detectable effect on the immunoprecipitation of CSPP-L (Figure 4B), suggesting that the interaction between these proteins is independent of these domains in UBR5 (transfection efficiency for these experiments is detailed in Supplemental Figure S3A). The interaction between UBR5 and CSPP-L was confirmed using GFP-tagged CSPP-L to coprecipitate endogenous UBR5 from HEK293T cells, but not with GFP-only control (Figure 4C). A significant amount of CSPP-L was still detectable in the nonbound fraction of GFP-UBR5 pull downs (Figure 4B), suggesting that UBR5 is not sequestering the complete pool of cellular CSPP-L in this assay.

The presence of higher molecular weight smears detected using anti–CSPP-L following pull down with GFP-UBR5 (Figure 4B) suggested the presence of polyubiquitylated forms of CSPP-L in HEK-293T cells. Probing with an anti-Ub antibody following pull down of GFP–CSPP-L confirmed the presence of ubiquitylated CSPP-L (CSPP-L-Ub) in HEK-293T cells (Figure 4C). To ensure the high molecular weight Ub smears were indeed covalently bound Ub, and not a ubiquitylated CSPP-L interactor, the GFP-CSPP-L co-IP was also performed using denaturing conditions (Figure 4C, far right). These presumptive polyubiquitylated forms of CSPP-L were attenuated in pull downs using the catalytically inactive form of UBR5 (HECT*), suggesting direct ubiquitylation of CSPP-L by UBR5 (Figure 4B and Supplemental Figure S3B). However, it should be noted that variation in *HECT interacting modified CSPP-L was observed between experiments, likely due to varied GFP-UBR5 transfection efficiency coupled with the presence of endogenous wild-type UBR5 (Supplemental Figure S3D). Despite this observation, a clear reduction in modified CSPP-L was observed interacting with *HECT when compared with

wild-type UBR5. Lower molecular weight CSPP-L species in WCE are likely degradation products of endogenous CSPP-L. Importantly, this experiment also confirmed the presence of ubiquitylated forms of endogenous CSPP-L (i.e., not GFP labeled). Overexpression of UBR5 did not alter total cellular CSPP-L levels (Supplemental Figure S3B), suggesting that UBR5-mediated ubiquitylation of CSPP-L is not targeting the protein for degradation by the proteasome.

UBR5 interacts with CSPP-L at the centriolar satellites

We confirmed that GFP-tagged UBR5 localizes to the nucleus and cytoplasm (Supplemental Figure S3A) and CSPP-L displays centrosomal and centriolar satellite localization (Supplemental Figure S3E, white arrows), consistent with previous reports (Patzke *et al.*, 2010). As UBR5 antibodies show cross-reactivity with cytoplasmic proteins by immunohistochemistry (unpublished data), we sought to further characterize the UBR5 and CSPP-L interaction in a cellular context using protein complementation assays to define subcellular localization. Bimolecular fluorescence complementation (BiFC) analysis (Figure 5A) indicated the presence of protein–protein interactions between CSPP-L and UBR5 in discrete perinuclear foci in HEK293T cells, consistent with the primary subcellular localization of CSPP-L to and around centrosomes (white arrows, Figure 5A). A similar subcellular distribution was observed for the BiFC signal generated by an interaction between CSPP-L and Ub (Figure 5A), suggesting that CSPP-L is ubiquitylated around the centrosome and consistent with our results above (Figure 4). A positive control assay between UBR5 and Ub showed strong nuclear and cytoplasmic foci (Figure 5A) consistent with the previously described localization of UBR5 to the nucleus and cytoplasm (Supplemental Figure S3A; Fuja *et al.*, 2004). Correct expression of V1- or V2-tagged BiFC fusion proteins was confirmed by immunoblotting for both the expression protein and the respective Venus fluorescent protein fragment (Figure 5B).

We next used BiFC to examine ubiquitylation of CSPP-L interaction pairs in hTERT-RPE1 cells and costained for PCM1 (which marks the centriolar satellites) to confirm detailed localization. A BiFC signal indicating Ub:CSPP-L was detected at the centrosome proximal centriolar satellites (Figure 5C), indicating that the perinuclear BiFC signal observed in HEK293T cells (Figure 5A) was indeed localized at centriolar satellites surrounding the centrosome. These data indicate that CSPP-L is ubiquitylated at the centriolar satellites.

UBR5 is necessary for efficient recruitment of CSPP-L to the centrosome and centriolar satellites

Consistent with the effects of UBR5 overexpression (Figure 4B), we observed no change in total cellular CSPP-L following UBR5 depletion by short-hairpin RNA (shRNA; Figure 6A). Further, we did not observe an accumulation of ubiquitylated CSPP-L following treatment with the proteasome inhibitor MG-132 (Supplemental Figure S3B). Together, these data strongly indicate that UBR5-mediated ubiquitylation of CSPP-L is not targeting the protein for degradation. Analysis of GFP-CSPP-L pull downs using chain-specific Ub antibodies indicated the presence of both K48- and K63-linked polyubiquitin chains on CSPP-L (Figure 6B). Nondegrading K63-linked polyubiquitin chains have been implicated in endocytosis trafficking and signal transduction (Ikeda and Dikic, 2008).

Interestingly, transiently coexpressed V1-CSPP-L and V2-Ub fusion proteins resulted in a BiFC signal that colocalized with PCM1 in hTERT-RPE1 cells (Figure 5C), indicating the presence of ubiquitylated CSPP-L at centriolar satellites. Moreover, the V1-CSPP-L:V2-Ub BiFC signal was confined to centriolar satellites (and likely the pericentriolar material) alone, because excessive ectopic (and endogenous) CSPP-L was detected at the cytoskeleton (microtubules [MTs] as inferred by Patzke *et al.*, 2006) by a CSPP-L–specific antibody (Figure 5D).

Depletion of UBR5 diminished localization of CSPP-L to the centrosome (Figure 6, C and E) and adjacent satellites as determined by a pericentriolar quantitation mask (Figure 6D). This effect was independent of disruption of centriolar satellites, as depletion of PCM1 did not prevent aggregation of CSPP-L at the centrosome (Figure 6C and Sternemalm *et al.*, unpublished data). Loss of PCM1 is known to disrupt centriolar satellite stability and ciliogenesis (Wang *et al.*, 2016), and accordingly PCM1 disruption depletes centriolar satellite accumulation of CSPP-L (Figure 6C). It is apparent that CSPP-L and UBR5 are integral to satellite stability, as depletion of either almost completely attenuates detectable PCM1 directly adjacent to the centrosome (Figure 6C).

DISCUSSION

We demonstrate a novel function for the E3 Ub ligase UBR5 in regulation of ciliogenesis via maintenance of centriolar satellite stability. We also demonstrate a novel protein–protein interaction between UBR5 and the CSPP-L isoform of CSPP1, predominantly at the centrosome and surrounding centriolar satellites. CSPP-L is an established positive regulator of ciliogenesis (Patzke *et al.*, 2010) and a prominent cilia-localizing protein (Mick *et al.*, 2015). Cilium assembly is tightly linked to exit from mitosis into G1 phase (Rieder *et al.*, 1979). CSPP-L is increasingly recruited to the centrosome during G2/prophase in cell cycle progression, and detected on spindle MTs during mitosis, concomitant with centriolar satellite dispersal (Patzke *et al.*, 2006; Kim *et al.*, 2016). This cell cycle–dependent localization of CSPP-L to the primary cilium and spindle apparatus is likely regulated via posttranslational regulatory mechanisms. Indeed, the UPS is a known regulator of centriolar satellite stability (Shearer and Saunders, 2016) and we observed that UBR5 is necessary to stabilize not only centriolar satellite organization, but also CSPP-L's centrosomal localization.

Another E3 ubiquitin ligase, MIB1, is also known to regulate ciliogenesis via ubiquitin-mediated regulation of PCM1 function (Villumsen *et al.*, 2013; Wang *et al.*, 2016). We observed a weak interaction between UBR5 and MIB1, but not between UBR5 and PCM1. This may indicate large multiprotein complexes arising at centriolar satellites but as these putative complexes would also presumably accumulate PCM1—a major component of centriolar satellites—this explanation is improbable (Kubo *et al.*, 1999). More likely, as UBR5 also interacts with γ-tubulin, the apparent weak interaction between UBR5 and MIB1 may reflect a general accumulation of UBR5 around the centrosome.

Even though we detected ubiquitylation of CSPP-L in association with UBR5, siRNA-mediated depletion of UBR5 did not alter cellular levels of CSPP-L, suggesting that UBR5 is not targeting CSPP-L for proteasomal degradation. BiFC experiments indicate that ubiquitinylated CSPP-L is primarily confined to centriolar satellites, while excessive and nonubiquitylated CSPP-L (i.e., not detected by BiFC for Ub:CSPP-L) localizes to MTs (Figure 5D). Notably, both K48- and K63-linked poly-Ub conjugated forms of CSPP-L were detected interacting with UBR5, indicating the presence of nondegrading Ub signaling events. UBR5 is known to assemble nondegrading ubiquitin chains on β-catenin (Hay-Koren *et al.*, 2011) and ATMIN (Zhang *et al.*, 2014). Nondegrading Ub signaling is also involved in other aspects of centriolar satellite maintenance. For example, MIB1 monoubiquitylates PCM1, AZI, and CEP290 in the absence of UV cellular stress and maintains these proteins in an inactive form until monoubiquitylation is reversed (Villumsen *et al.*, 2013). However, another study found PCM1 to be degraded by MIB1-mediated polyubiquitylation (Wang *et al.*, 2016) with discrepancies in results

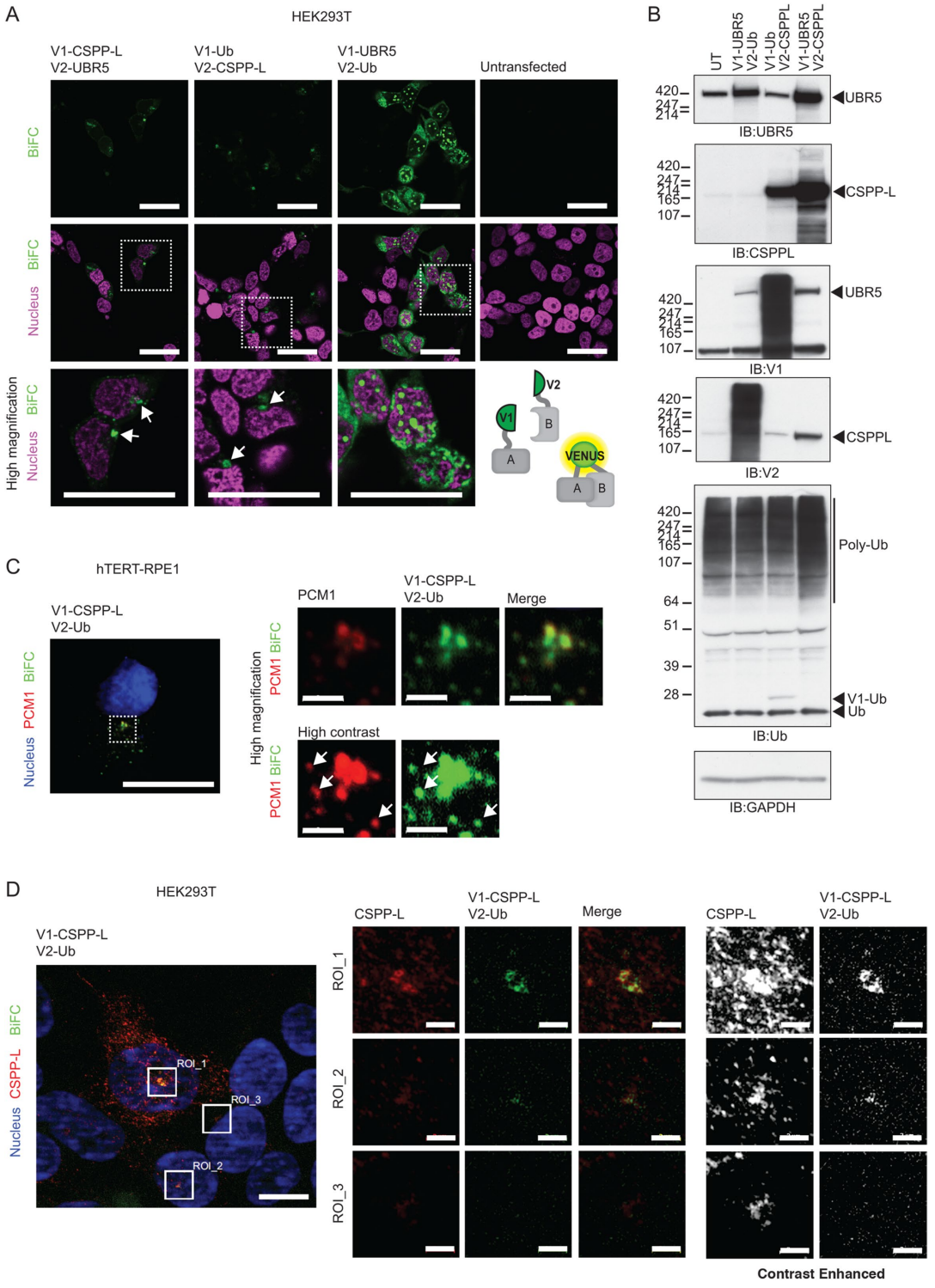

FIGURE 5: UBR5 interacts with CSPP-L at the centrosome. (A) Left to right, CSPP-L interacts with UBR5 in large foci adjacent to the nucleus (arrows). CSPP-L interacts with Ub in large foci adjacent to the nucleus (arrows). Interaction between UBR5 and Ub in HEK293T cells shows nuclear and cytoplasmic localization, with large foci of UBR5 and Ub in the nucleus. Untransfected cells show no visible signal. Nuclear marker is H2B-mCherry (magenta). High-powered inset fields are indicated by a dashed box (bar = 30 μm) and schematic of BiFC analysis for protein–protein interactions included. Data are representative of two experiments. (B) Immunoblot data showing correct production of fusion proteins in BiFC assay. Expected fusion protein sizes are V2-CSPP-L 152 kDa, V1-UBR5 329 kDa, V1-Ub 28 kDa, and V2-Ub 19 kDa. (C) CSPP-L/Ub interacting pairs colocalize with PCM1 (centriolar satellite marker) in hTERT-RPE1 cells. Bar = 20 μm. High magnification of ROI bar = 2 μm. (D) High-level expression of CSPP-L/Ub BiFC vectors shows CSPP-L and Ub interaction is confined to the centriolar satellites, despite strong detection of CSPP-L at the MTs in HEK293T cells. Region of interest (ROI) 1 shows relatively high BiFC pair expression, ROI 2 shows relatively low BiFC pair expression, and ROI 3 shows no BiFC pair expression. Bar = 10 μm. High magnification of ROI bar = 2 μm.

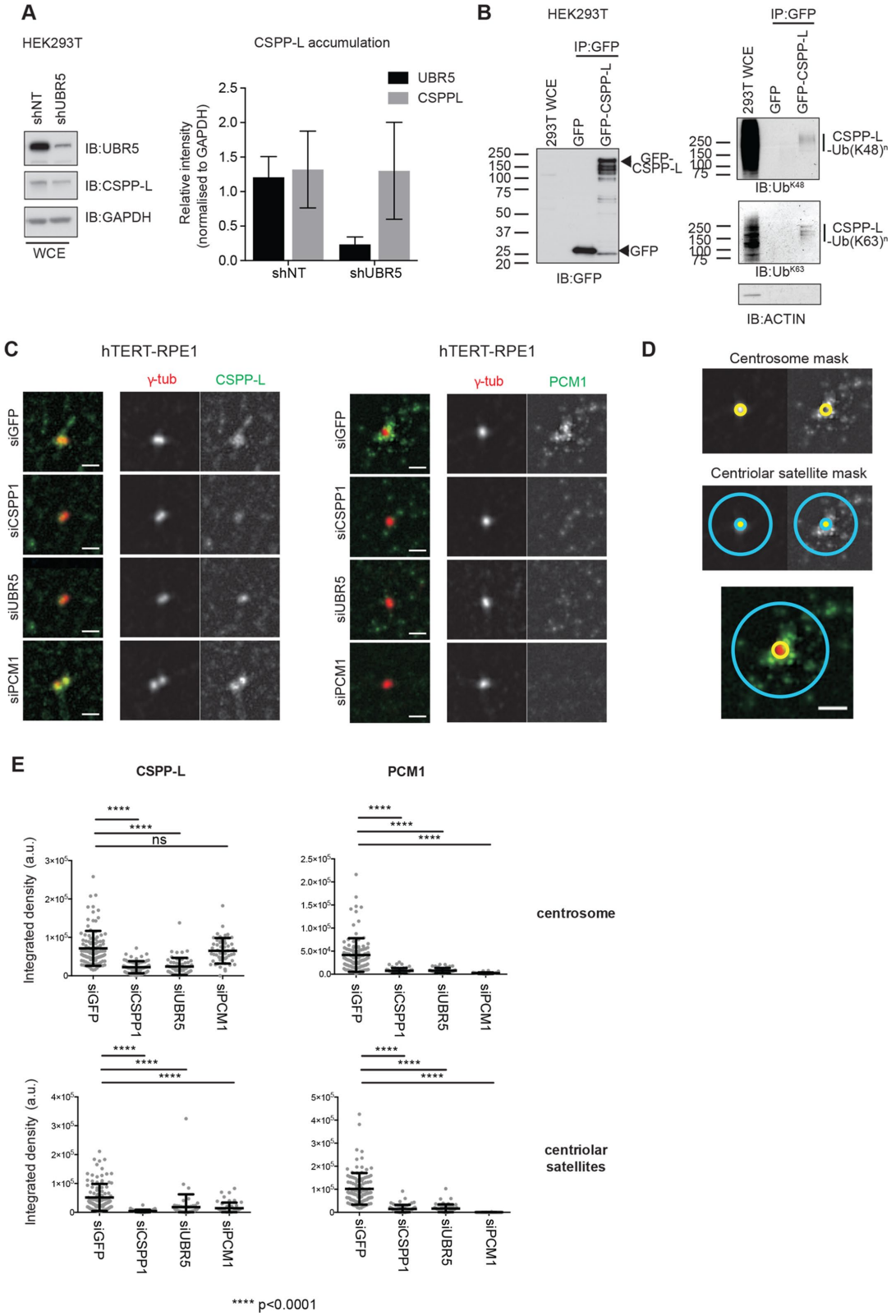

FIGURE 6: UBR5 maintains CSPP-L at the centrosome/centriolar satellites, and is required for centriolar satellite stability. (A) Depletion of UBR5 by shRNA in HEK293T cells does not decrease CSPP-L levels. shRNA induced with 1 μg/ml doxycycline 48 h before harvest. Data summary represents results from four independent experiments; $n = 6$ replicates per experiment. (B) Immunoprecipitation of GFP-CSPP-L coimmunoprecipitates CSPP-L–bound lysine-48 (K48) linked Ub chains and lysine-63 (K63) linked Ub chains. Transfections performed 24 h before harvest. (C) Depletion of UBR5 (but not PCM1) causes dispersion of centrosomal CSPP-L in RPE1 cells. (D) Centrosome/centriolar satellite mask. (E) Quantitation of loss of CSPP-L/PCM1 at the centrosome according to the mask described in D. At least 30 cells were scored per sample and statistical analysis performed using two-tailed *t* test.

likely due to different methodologies used in each study (Shearer and Saunders, 2016). Depletion of either CSPP-L or UBR5 disrupted centriolar satellite organization (as defined by PCM1), indicating that UBR5-mediated ubiquitylation of CSPP-L promotes localization of CSPP-L to centriolar satellites. The UBR5/CSPP-L interplay is a potential regulatory mechanism controlling the timely release and activity of ciliogenesis promoting factors, including CSPP-L itself; however, further study is required to confirm this model. Further work should also examine CSPP-L interactors for other significant E3 Ub ligase enzymes, as K48-linked Ub chains detected on CSPP-L may not be generated by UBR5 and there is significant redundancy and multiplicity in the UPS (Iconomou and Saunders, 2016).

Primary cilia are an important component of the Hh signal transduction pathway during development (Rohatgi *et al.*, 2007; Goetz and Anderson, 2010) and autocrine Hh signaling is reactivated in some cancer types (Kubo *et al.*, 2004; Liu *et al.*, 2014; Ertao *et al.*, 2016). Several studies have implicated UBR5 as a modulator of Hh signaling and a variety of model organisms with *UBR5* mutations display developmental defect phenotypes. Hence, it is worth considering a potential underlying role for UBR5 in Hh signaling via the novel role in regulating ciliogenesis.

Mutations in the *Drosophila* orthologue of UBR5 (Hyd) display a range of severe developmental phenotypes (reviewed in Shearer and Saunders, 2016). Specifically, Hyd directly regulates Hh and Dpp signaling (Lee *et al.*, 2002) and can also indirectly affect Hh signal transduction by regulating Ci promoter binding (Wang *et al.*, 2014). *Ubr5*-null mouse embryos die at midgestation due to failure of yolk sac vascular development (Saunders *et al.*, 2004). Coincidently, this timing corresponds to the developmental stage at which primary cilia first appear on epiblast-derived mesothelial and endothelial cells (Bangs *et al.*, 2015). Conditional deletion of *Ubr5* in the early embryonic limb-bud mesenchyme of mice resulted in decreased Hh ligand production and decreased Hh pathway activity (Kinsella *et al.*, 2016). It was not determined whether these effects on Hh signaling were direct (cell autonomous) or indirect (noncell autonomous) and so the underlying mechanism for this effect remains elusive. UBR5 has not been shown to directly bind Hh pathway components in human cells apart from GLI2 (Moncrieff *et al.*, 2015); however, multiple Hh pathway components including PTCH1, GLI1, and HHIP are direct transcriptional targets of active Hh signaling (Gupta *et al.*, 2010). It cannot be excluded that a reduction in general Hh activity with reduced UBR5 may indicate a more general disruption in signal transduction caused by failed ciliogenesis.

From a disease perspective, UBR5 has not been specifically examined in the context of ciliopathies. Rare *UBR5* missense mutations have been linked to familial epilepsy (Kato *et al.*, 2012) and cilia have been implicated in some forms of epilepsy (Delgado-Escueta, 2007), but this link is speculative. Exome sequencing data from the Exome Aggregation Consortium (ExAC) demonstrates a very low loss of function (LoF) mutation rate for *UBR5* in healthy somatic tissue. Only four LoF *UBR5* variants were observed, with a very low frequency (Lek *et al.*, 2016). These indicate strong selective pressure against deactivating *UBR5* mutations and support a critical role for UBR5 in human development, consistent with observations in model organisms.

Correlated expression of *CSPP1* and *UBR5* mRNA in human cancer cell lines and primary breast cancer gives additional relevance of CSPP-L and UBR5 in normal and transformed mammary epithelium. However, further work is required to confirm whether UBR5/CSPP-L signaling is mechanistically responsible for cilia maintenance, and to understand the putative impact of epithelial lineage-specific expression of CSPP1 isoforms (which cannot be distinguished by mRNA expression data) and their coexpression and interaction with UBR5 (Sternemalm *et al.*, 2014). It is interesting to note that ciliary Hh signaling controls branching morphology of mammary gland xenografts (McDermott *et al.*, 2010) and the Hh signaling pathway is a growth-promoting factor for breast cancer subgroups (Kubo *et al.*, 2004; O'Toole *et al.*, 2011). Future analysis may focus on determining putative correlations between UBR5 controlled cilia formation and mammary epithelial cell differentiation and transformation.

In summary, we have demonstrated a highly novel role for the E3 Ub ligase UBR5 in primary cilia maintenance/formation, with potential implications for understanding the molecular basis of key signaling pathways in development and disease.

MATERIALS AND METHODS

Gene expression correlation

Global gene expression correlation in the NCI-60 panel of cancer cell lines ($n = 60$; Stinson *et al.*, 1992) was analyzed using the Pattern comparison tool from CellMiner (Reinhold *et al.*, 2012). Expression intensity Z-scores for 26,065 genes were correlated against *UBR5* expression based on Affymetrix microarray transcript intensity level and significance determined using Pearson's correlation coefficient with $p < 0.05$ without multiple comparisons. Linear-regression analysis was performed comparing intensity Z-scores for *UBR5* and *CSPP1* expression using data obtained from the Cross-correlations tool from CellMiner. Coexpression data was validated using TCGA (Ciriello *et al.*, 2015), CCCLE (Barretina *et al.*, 2012), and Molecular Taxonomy of Breast Cancer International Consortium (METABRIC; Curtis *et al.*, 2012) cohorts. Analyses were performed using cBIOPortal (Cerami *et al.*, 2012; Gao *et al.*, 2013). Coexpression measured on mRNA expression determined using RNA-seq data (Z-score, threshold +/–2.0). Analysis of genes coexpressed with *CSPP1* in 1671 datasets representing all major cancer types was performed using the SEEK database (Zhu *et al.*, 2015b).

Plasmids

Full-length *UBR5* ORF was obtained from pEGFP-C1 *EDD* (#37190; Addgene, Cambridge, MA; Henderson *et al.*, 2002) and used to create pENTR221-*UBR5* (Addgene; #81062). *UBR5* cDNA was digested from pEGFP-C1 *EDD* and was cloned into pENTR221 containing synthetic fragments (GeneArt, Life Technologies, Carlsbad, CA) of the 5′ and 3′ region (base pairs 1–1129 and 6933–8404, respectively) of *UBR5*. Mutagenesis of *UBR5* was achieved by subcloning synthetic fragments (GeneArt, Life Technologies) of the HECT domain (base pairs 6933–8404) with a mutation (base pairs t8302g and g8303c) corresponding to C2768A (UBR5^{C2768A}, herein HECT*; Addgene; #81065), the *UBR5* MLLE domain (Kozlov *et al.*, 2007) (base pairs 6933–8404) with mutations (base pairs t7204g, a7205c, t7206c, a7243g, a7244c, and a7245c) corresponding to Y2402A and K2415A (UBR5$^{Y2402A/K2415A}$, herein MLLE*; Addgene; #81064), and the UBR domain (base pairs 3163–4217) with a mutation (base pair g3704t) corresponding to W1235L (UBR5^{W1235L}, herein UBR*; Addgene; #81063). A Gateway entry vector encoding full-length *CSPP-L* was generated by PCR using modified flanking primers and the previously described pCSPP-L-EGFP vector (Patzke *et al.*, 2006).

Gateway entry vectors were used to generate expression clones using the following destination vectors: Vivid Colors pcDNA 6.2/N-EmGFP-DEST (V356-20; Invitrogen, Carlsbad, CA), BiFC vectors pDEST-V1-ORF (Addgene; #73635), and pDEST-V2-ORF (Addgene; #73636; Croucher *et al.*, 2016). GFP-UBR5 (Addgene; #52050) and GFP-UBR5 HECT* (Addgene; #52051) expression vectors are described (Gudjonsson *et al.*, 2012). V1-Ub and V2-Ub expression vectors are described (Lee *et al.*, 2015). Recombination was

catalyzed by Gateway LR clonase II enzyme mix (11791-020; Invitrogen) according to manufacturer's instructions.

shRNA sequences to *UBR5* were obtained from the RNAi codex project (Olson *et al.*, 2006). Hairpins were cloned into pEN_TmiRc3 (Addgene; #25748), before shuttling into pSLIK Gateway compatible expression vectors encoding Venus (Addgene; #25734) or G418 (Addgene; #25735) selectable markers as described (Shin *et al.*, 2006). The hairpin sequence 5′-CGCAGTGAATGTAGATTCCAAA-3′ (HP_6400, herein shUBR5; Addgene; #81066) was found to efficiently silence UBR5 and was used for experiments. A scrambled sequence 5′-TCGATGCTCTAAGGTTCTATC-3′ (herein shNT; Addgene; #81067) was used as a nontargeting control. pLV-CCN-H2B-mCherry was a kind gift from Marc Giry-Laterriere (Kinghorn Cancer Centre).

PAGE and immunoblot

All lysates were made using RIPA buffer supplemented with protease inhibitors (1183617001; Roche Diagnostics, Basel, Switzerland), and 10 mM *N*-ethylmaleimide (E3876-5G; Sigma-Aldrich, St. Louis, MO). Where indicated, denaturing lysis was performed using freshly prepared 8 M Urea lysis buffer supplemented with 10% glycerol (vol/vol), 20% SDS (wt/vol), 5 nM dithiothreitol, and 10 mM Tris (pH 6.8). Cultured cells were washed with phosphate-buffered saline (PBS) and scraped from culture vessels in the presence of lysis buffer on ice. Lysates were cleared by centrifugation at 4°C and the total protein concentration determined using protein assay dye reagent (500-0006; Bio-Rad, Hercules, CA) according to manufacturer's instructions. Denaturing lysates were sonicated before clearing. Samples were separated using SDS–PAGE, transferred to Immobilon-P PVDF 0.45 µm membrane (IPVH00010; Merck Millipore, Darmstadt, Germany) and subsequently immunoblotted using standard procedure. Densitometry was performed using ImageJ. Lane density was plotted and relative band intensity determined by area under curve analysis. Densitometry was restricted to a comparison of lanes from the same exposure and run on the same gel. Intensity was normalized to loading control and was standardized to the first lane of each gel. The theoretical size of fusion proteins was calculated using the Compute pI/Mw tool available on the ExPASy server (Bjellqvist *et al.*, 1993) via the average resolution setting.

The following antibodies were used for immunoblotting: goat anti-EDD N-19 (sc-9561; Santa Cruz, Dallas, TX) diluted 1:5000; rabbit anti-EDD1 (A300-573A; Bethyl Laboratories, Montgomery, TX) diluted 1:5000; rabbit anti-CSPP1 (binds CSPP-L only; 11931-1-AP; Proteintech, Manchester, UK) diluted 1:5000; rabbit anti-PCM1 (ab72443; Abcam, Cambridge, UK) diluted 1:5000; mouse anti-GFP (MMS-118P; Covance, Princeton, NJ) diluted 1:5000; mouse anti-GFP (11814460001; Roche Diagnostics) diluted 1:5000; rabbit anti-ubiquitin (ab7780; Abcam) diluted 1:2000; mouse anti–β-ACTIN (A5441; Sigma-Aldrich) diluted 1:5000; mouse anti-GAPDH (ACR110PT; Acris-Antibodies) diluted 1:10,000; rabbit anti-ubiquitin (ab7780; Abcam) diluted 1:2000; rabbit anti-ubiquitin (linkage-specific K48; ab140601; Abcam) diluted 1:5000; rabbit anti-ubiquitin (linkage-specific K63; ab179434; Abcam) diluted 1:5000; rabbit anti–γ-tubulin (T3320; Sigma-Aldrich) 1:5000; mouse anti–γ-tubulin (T6557; Sigma-Aldrich) diluted 1:5000; and rabbit anti-CEP290 (ab85728; Abcam) diluted 1:2000. All antibodies were diluted in 5% (wt/vol) bovine serum albumin Tris-buffered saline solution.

Immunoprecipitation

GFP-tagged fusion proteins were isolated from whole cell extract (WCE) using GFP-Trap (GTA-100; Chromotek, Planegg-Martinsried, Germany) affinity purification reagent according to manufacturer's instructions. In brief, 20 µl of bead slurry was washed twice in 10 mM Tris-HCl (pH 7.5) with 150 mM NaCl and 0.5 mM EDTA before addition of 250 µg WCE. Samples were incubated for 1 h at room temperature with gentle end-over-end mixing. Beads were washed twice, and bound proteins eluted by heating at 95°C for 10 min in 1× SDS gel loading dye.

Cell culture

The following cell lines were cultured at 37°C with 5% CO_2 and passaged according to American Type Culture Collection (ATCC, Manassas, VA) recommendations. Cell line identity was verified using standard in-house authentication. hTERT-RPE1 (CRL-4000; ATCC) human hTERT immortalized retina pigmented epithelial cells were maintained in DMEM-F12 culture medium (31331-028; Life Technologies) supplemented with 10% fetal bovine serum (FBS; vol/vol; 10270-106; Life Technologies) and 1% penicillin–streptomycin solution (vol/vol; P4333; Sigma-Aldrich). Human embryonic kidney (HEK293T; CRL-3216, ATCC) cells were grown using DMEM culture medium (11995-065; Life Technologies) supplemented with 10% FBS (vol/vol), MEM nonessential amino acids (11140-050; Life Technologies), and sodium pyruvate (11360-070; Life Technologies). MDA-MB-231 (HTB-26; ATCC) human mammary carcinoma cells were grown with RPMI 1640 culture medium (11875-085; Life Technologies) supplemented with 10% (vol/vol) FBS, 10 mM HEPES buffer (15630-080; Life Technologies), and 0.2 IU/ml human insulin (Actrapid Penfill; Novo Nordisk). Inhibition of proteasomal degradation was achieved where indicated using 10 µM MG-132 (474790-1MG; Calbiochem) in complete growth media before harvest.

HEK293T cells expressing H2B-mCherry were generated by stable transduction of pLV-CCN-H2B-mCherry viral supernatant. Cells expressing H2B-mCherry were grown under 500 µg/ml G418 selection and sorted for moderate expression as described (McCloy *et al.*, 2014). HEK293T cells expressing a short hairpin to UBR5 (shUBR5) or a nontargeting scrambled control (shNT) were generated by stable transduction of pSLIK (see above) viral supernatant. Viral transduction to achieve minimal multiplicity of infection (MOI) performed visually in serial dilution as described (Shearer and Saunders, 2015). Sorting was performed by Garvan Flow Cytometry Facility staff.

Plasmid transfections were performed using Xtreme Gene 9 HP transfection reagent (06366236001; Roche). Cells were plated out 24 h before achieving roughly 50% confluency at the time of transfection. Plasmid DNA was mixed with transfection reagent in a 1:3 (µg DNA:µl reagent) ratio, diluted in a total volume of 100 µl Opti-Mem I reduced serum media (31985-070; Life Technologies). Complexes were incubated for 15 min at room temperature before being added to cells with complete growth media. Transient gene silencing in HEK293T cells using siRNA was performed using lipofectamine 2000 (11668019; Life Technologies) according to manufacturer's instructions. 5×10^5 cells were plated in a six-well plate 24 h before transfection. siRNA (25 pmol) was combined with 7 µl transfection reagent diluted in 100 µl total volume. After plating, cells were subject to imaging for proliferation assay (see below) before harvest and lysis at 24–48 h as indicated. Epifluorescence imaging was performed using a Leica DM550 microscope.

Ciliogenesis assay

Cells (5×10^4) were seeded on high precision glass coverslips (0.17 ± 0.01 mm; 1014/10; Hecht Assistent, Sondheim/Rhön, Germany) in 30-mm wells, allowed to adhere overnight, and transfected with siRNA using RNAiMAX (13778-150; Life Technologies) for transient gene silencing. Posttransfection (48 h) cells were washed twice in serum-free DMEM-F12 and cilia formation induced by continued

incubation in serum-free medium for 48 h. For cilia detection, cells were fixed in methanol (–20°C) and stained subsequently with a glutamylated tubulin–specific mouse monoclonal antibody (clone GT335, AG-20B-0020-C100; Adipogen San Diego, CA) and a mouse-specific Cy3 labeled secondary antibody (715-165-151; Jackson Immuno Research, West Grove, PA) for labeling of ciliary axonemes. At least 150 cells were scored by manual inspection on an AxioImagerZ.1 epifluorescence microscope equipped with a 40×/NA 0.95 and a 63×/NA 1.4 Plan-Apochromat lens and a HXP120 Metal-Halide Illuminator (Carl Zeiss, Jena, Germany).

Immunofluorescence microscopy

Cells were grown on heat-sterilized cover glasses (0.17 ± 0.01 mm; 1014/10; Hecht Assistent), fixed for 15 min in 1% neutral buffered formalin solution at room temperature before postfixation in methanol (–20°C). Cells were rehydrated for IFM staining by three consecutive washes in PBS and blocked and permeabilized for 15 min in PBS-AT (PBS containing 5% wt/vol bovine serum albumin [A4503; Sigma-Aldrich] and 0.1% vol/vol Triton X-100 [T9284; Sigma-Aldrich]). Cells were stained with primary antibodies for 2 h at room temperature, washed three times in PBS, and stained with secondary antibodies for 1 h. All antibody incubations were performed in PBS-AT. Cells were washed three times in PBS, counterstained for DNA (Hoechst 33258 in PBS; 14530; Sigma-Aldrich), washed briefly in distilled water, dried, and mounted on object glasses using Prolong Gold (P36930; Life Technologies). Fluorescence images were acquired using appropriate optical filters on a multifluorescent bead calibrated AxioImager Z1 ApoTome microscope system (Carl Zeiss) equipped with a 100× or a 63× lens (both PlanApo, NA 1.4) and an AxioCam MRm camera. To display the entire cell volume, images are presented as maximal projections of z-stacks using Axiovision 4.8.2 (Carl Zeiss).

Images for quantitative IFM imaging were acquired on a multifluorescence submicron beads calibrated CellObserver microscope system (Carl Zeiss) equipped with a 40×/1.3 PlanApo Phase 3 lens and an AxioCam MRm camera. Images were acquired with constant exposure times at 10 random positions per coverslip and in seven optical sections at 0.5 µm distance, centered around focal planes for cilia. Central focal planes were identified by γ-tubulin labeling as centrosome reference using a contrast-based autofocus routine (AxioVision 4.8.2). Image analysis was performed in Fiji/ImageJ (Schindelin *et al.*, 2012). Sum projections of individual channels were background corrected using a 5 pixel rolling circle algorithm and segmented by signal intensity and morphological thresholds. Thresholded γ-tubulin signals defined the centrosome compartment mask. The radius of the centrosome area was iteratively dilated (20×) to cover the pericentrosomal area, and subtracted for the core centrosomal area to create the centriolar satellite mask. Fluorescence signal intensities in thresholded areas under each mask were measured in all channels to obtain integrated signal intensities.

The following antibodies were used for immunofluorescence: rabbit anti-PCM1 (ab72443; Abcam) diluted 1:1000; mouse anti–γ-tubulin (T6557; Sigma-Aldrich) diluted 1:500; rabbit anti-CSPP1 (binds CSPP-L only; 11931-1-AP; Proteintech) diluted 1:500; and mouse anti–glutamylated tubulin (GT335; Enzo Life Sciences) diluted 1:500. All statistical analyses were performed using Prism (Graphpad Software).

BiFC

BiFC allows fluorescence visualization of binary protein–protein interactions (Kerppola, 2008). Proteins of interest were expressed fused to either Met^{1}-Gln^{157} (V1) or Lys^{158}-Lys^{238} (V2) separated by a 2× GGGGS linker sequence (Croucher *et al.*, 2016). Recombination of the Venus fluorescent protein indicates a positive interaction. A total of 5×10^5 HEK293T cells (containing stable H2B-mCherry) were plated in a six-well plate containing a round coverslip 24 h before transfection. Cells were transfected with 500 ng of each plasmid construct (see above) and incubated for 18 h before coverslips were mounted with Vectashield mounting medium (H-1400; Vector Laboratories, Burlingame, CA). Remaining cells were harvested for immunoblot analysis to ensure correct fusion protein translation. Confocal imaging was performed using a Leica TCS SP8 confocal microscope optimized for at least 75 nm resolution. Gain and resolution were maintained across all samples within experiments. Fluorescent images were pseudocolored with an appropriate lookup table (LUT) and merged using ImageJ.

Flow cytometry

hTERT RPE1 cells (2×10^5) were seeded in 60-mm dishes and reverse transfected with siRNA using lipofectamine RNAiMAX (13778-150; Invitrogen). Asynchronous samples were harvested 48 h post-transfection, while serum-starved samples were washed three times with serum-free medium and starved 48 h before harvest 96 h post-transfection. Cells were stained with Pacific Orange (P30253; Invitrogen) for live/dead labeling before ice-cold methanol fixation. Mitotic cells were labeled using antibody against phospho-histone H3 (06-570; Merck) and a rabbit-specific R-phycoerythrin (PE) antibody (P2771MP; Life Technology) secondary. DNA were stained using FxCycle FarRed (F10348; Invitrogen) and RNaseA (12091-021; Invitrogen). Samples were run on a LSRII flow cytometer with BD FACSdiva software and further analyzed using FlowJo v10 (BD Biosciences, San Jose, CA).

ACKNOWLEDGMENTS

This research was supported by funding from the National Health and Medical Research Council of Australia (project grant GNT1052963), Cancer Institute New South Wales (10/FRL/3-02), the Mostyn Family Foundation, the Australian Government Department of Innovation, Industry, Science and Research, Oslo University Hospital, and Radiumhospitalets Legater. R.F.S. is the recipient of an Australian Government Research Training Program Scholarship and the Baxter Family Scholarship. S.P. is the recipient of a Career Development Fellowship from the Norwegian Cancer Society. D.N.S. and A.B. are recipients of a Patricia Helen Guest Fellowship.

REFERENCES

Akizu N, Silhavy JL, Rosti RO, Scott E, Fenstermaker AG, Schroth J, Zaki MS, Sanchez H, Gupta N, Kabra M, *et al.* (2014). Mutations in CSPP1 lead to classical Joubert syndrome. Am J Hum Genet 94, 80–86.

Asiedu M, Wu D, Matsumura F, Wei Q (2009). Centrosome/spindle pole-associated protein regulates cytokinesis via promoting the recruitment of MyoGEF to the central spindle. Mol Biol Cell 20, 1428–1440.

Bangs FK, Schrode N, Hadjantonakis AK, Anderson KV (2015). Lineage specificity of primary cilia in the mouse embryo. Nat Cell Biol 17, 113–122.

Barretina J, Caponigro G, Stransky N, Venkatesan K, Margolin AA, Kim S, Wilson CJ, Lehar J, Kryukov GV, Sonkin D, *et al.* (2012). The Cancer Cell Line Encyclopedia enables predictive modelling of anticancer drug sensitivity. Nature 483, 603–607.

Bjellqvist B, Hughes GJ, Pasquali C, Paquet N, Ravier F, Sanchez JC, Frutiger S, Hochstrasser D (1993). The focusing positions of polypeptides in immobilized pH gradients can be predicted from their amino acid sequences. Electrophoresis 14, 1023–1031.

Boldt K, van Reeuwijk J, Lu Q, Koutroumpas K, Nguyen TM, Texier Y, van Beersum SE, Horn N, Willer JR, Mans DA, *et al.* (2016). An organelle-specific protein landscape identifies novel diseases and molecular mechanisms. Nat Commun 7, 11491.

Cajanek L, Glatter T, Nigg EA (2015). The E3 ubiquitin ligase Mib1 regulates Plk4 and centriole biogenesis. J Cell Sci 128, 1674–1682.

Callaghan MJ, Russell AJ, Woollatt E, Sutherland GR, Sutherland RL, Watts CK (1998). Identification of a human HECT family protein with homology to the *Drosophila* tumor suppressor gene hyperplastic discs. Oncogene 17, 3479–3491.
Cerami E, Gao J, Dogrusoz U, Gross BE, Sumer SO, Aksoy BA, Jacobsen A, Byrne CJ, Heuer ML, Larsson E, *et al.* (2012). The cBio cancer genomics portal: an open platform for exploring multidimensional cancer genomics data. Cancer Discov 2, 401–404.
Ciehanover A, Hod Y, Hershko A (1978). A heat-stable polypeptide component of an ATP-dependent proteolytic system from reticulocytes. Biochem Biophys Res Commun 81, 1100–1105.
Ciriello G, Gatza ML, Beck AH, Wilkerson MD, Rhie SK, Pastore A, Zhang H, McLellan M, Yau C, Kandoth C, *et al.* (2015). Comprehensive molecular portraits of invasive lobular breast cancer. Cell 163, 506–519.
Clancy JL, Henderson MJ, Russell AJ, Anderson DW, Bova RJ, Campbell IG, Choong DY, Macdonald GA, Mann GJ, Nolan T, *et al.* (2003). EDD, the human orthologue of the hyperplastic discs tumour suppressor gene, is amplified and overexpressed in cancer. Oncogene 22, 5070–5081.
Croucher DR, Iconomou M, Hastings JF, Kennedy SP, Han JZ, Shearer RF, McKenna J, Wan A, Lau J, Aparicio S, Saunders DN (2016). Bimolecular complementation affinity purification (BiCAP) reveals dimer-specific protein interactions for ERBB2 dimers. Sci Signal 9, ra69.
Curtis C, Shah SP, Chin SF, Turashvili G, Rueda OM, Dunning MJ, Speed D, Lynch AG, Samarajiwa S, Yuan Y, *et al.* (2012). The genomic and transcriptomic architecture of 2,000 breast tumours reveals novel subgroups. Nature 486, 346–352.
Delgado-Escueta AV (2007). Advances in genetics of juvenile myoclonic epilepsies. Epilepsy Curr 7, 61–67.
Eisen MB, Spellman PT, Brown PO, Botstein D (1998). Cluster analysis and display of genome-wide expression patterns. Proc Natl Acad Sci USA 95, 14863–14868.
Ertao Z, Jianhui C, Chuangqi C, Changjiang Q, Sile C, Yulong H, Hui W, Shirong C (2016). Autocrine Sonic hedgehog signaling promotes gastric cancer proliferation through induction of phospholipase Cγ1 and the ERK1/2 pathway. J Exp Clin Cancer Res 35, 63.
Fuja TJ, Lin F, Osann KE, Bryant PJ (2004). Somatic mutations and altered expression of the candidate tumor suppressors *CSNK1ε, DLG1,* and *EDD/hHYD* in mammary ductal carcinoma. Cancer Res 64, 942–951.
Gao J, Aksoy BA, Dogrusoz U, Dresdner G, Gross B, Sumer SO, Sun Y, Jacobsen A, Sinha R, Larsson E, *et al.* (2013). Integrative analysis of complex cancer genomics and clinical profiles using the cBioPortal. Sci Signal 6, pl1.
Goetz SC, Anderson KV (2010). The primary cilium: a signalling centre during vertebrate development. Nat Rev Genet 11, 331–344.
Gudjonsson T, Altmeyer M, Savic V, Toledo L, Dinant C, Grofte M, Bartkova J, Poulsen M, Oka Y, Bekker-Jensen S, *et al.* (2012). TRIP12 and UBR5 suppress spreading of chromatin ubiquitylation at damaged chromosomes. Cell 150, 697–709.
Gupta GD, Coyaud E, Goncalves J, Mojarad BA, Liu Y, Wu Q, Gheiratmand L, Comartin D, Tkach JM, Cheung SW, *et al.* (2015). A dynamic protein interaction landscape of the human centrosome-cilium interface. Cell 163, 1484–1499.
Gupta S, Takebe N, Lorusso P (2010). Targeting the Hedgehog pathway in cancer. Ther Adv Med Oncol 2, 237–250.
Hay-Koren A, Caspi M, Zilberberg A, Rosin-Arbesfeld R (2011). The EDD E3 ubiquitin ligase ubiquitinates and up-regulates β-catenin. Mol Biol Cell 22, 399–411.
Henderson MJ, Russell AJ, Hird S, Munoz M, Clancy JL, Lehrbach GM, Calanni ST, Jans DA, Sutherland RL, Watts CK (2002). EDD, the human hyperplastic discs protein, has a role in progesterone receptor coactivation and potential involvement in DNA damage response. J Biol Chem 277, 26468–26478.
Hershko A, Ciechanover A, Rose IA (1981). Identification of the active amino acid residue of the polypeptide of ATP-dependent protein breakdown. J Biol Chem 256, 1525–1528.
Hori A, Toda T (2017). Regulation of centriolar satellite integrity and its physiology. Cell Mol Life Sci 74, 213–229.
Iconomou M, Saunders DN (2016). Systematic approaches to identify E3 ligase substrates. Biochem J 473, 4083–4101.
Ikeda F, Dikic I (2008). Atypical ubiquitin chains: new molecular signals. 'Protein modifications: beyond the usual suspects' review series. EMBO Rep 9, 536–542.
Inoko A, Matsuyama M, Goto H, Ohmuro-Matsuyama Y, Hayashi Y, Enomoto M, Ibi M, Urano T, Yonemura S, Kiyono T, *et al.* (2012). Trichoplein and Aurora A block aberrant primary cilia assembly in proliferating cells. J Cell Biol 197, 391–405.
Johnson D (2014). The ubiquitin-proteasome system: opportunities for therapeutic intervention in solid tumors. Endocr Relat Cancer 22, T1–T17.
Kasahara K, Kawakami Y, Kiyono T, Yonemura S, Kawamura Y, Era S, Matsuzaki F, Goshima N, Inagaki M (2014). Ubiquitin-proteasome system controls ciliogenesis at the initial step of axoneme extension. Nat Commun 5, 5081.
Kato T, Tamiya G, Koyama S, Nakamura T, Makino S, Arawaka S, Kawanami T, Tooyama I (2012). UBR5 gene mutation is associated with familial adult myoclonic epilepsy in a Japanese family. ISRN Neurol 2012, 508308.
Kerppola TK (2008). Bimolecular fluorescence complementation (BiFC) analysis as a probe of protein interactions in living cells. Annu Rev Biophys 37, 465–487.
Kim JH, Ki SM, Joung JG, Scott E, Heynen-Genel S, Aza-Blanc P, Kwon CH, Kim J, Gleeson JG, Lee JE (2016). Genome-wide screen identifies novel machineries required for both ciliogenesis and cell cycle arrest upon serum starvation. Biochim Biophys Acta 1863, 1307–1318.
Kim J, Lee JE, Heynen-Genel S, Suyama E, Ono K, Lee K, Ideker T, Aza-Blanc P, Gleeson JG (2010). Functional genomic screen for modulators of ciliogenesis and cilium length. Nature 464, 1048–1051.
Kim K, Rhee K (2011). The pericentriolar satellite protein CEP90 is crucial for integrity of the mitotic spindle pole. J Cell Sci 124, 338–347.
Kinsella E, Dora N, Mellis D, Lettice L, Deveney P, Hill R, Ditzel M (2016). Use of a conditional *Ubr5* mutant allele to investigate the role of an N-end rule ubiquitin-protein ligase in Hedgehog signalling and embryonic limb development. PLoS One 11, e0157079.
Kozlov G, Menade M, Rosenauer A, Nguyen L, Gehring K (2010). Molecular determinants of PAM2 recognition by the MLLE domain of poly(A)-binding protein. J Mol Biol 397, 397–407.
Kozlov G, Nguyen L, Lin T, De Crescenzo G, Park M, Gehring K (2007). Structural basis of ubiquitin recognition by the ubiquitin-associated (UBA) domain of the ubiquitin ligase EDD. J Biol Chem 282, 35787–35795.
Kubo M, Nakamura M, Tasaki A, Yamanaka N, Nakashima H, Nomura M, Kuroki S, Katano M (2004). Hedgehog signaling pathway is a new therapeutic target for patients with breast cancer. Cancer Res 64, 6071–6074.
Kubo A, Sasaki H, Yuba-Kubo A, Tsukita S, Shiina N (1999). Centriolar satellites: molecular characterization, ATP-dependent movement toward centrioles and possible involvement in ciliogenesis. J Cell Biol 147, 969–980.
Lee JD, Amanai K, Shearn A, Treisman JE (2002). The ubiquitin ligase Hyperplastic discs negatively regulates *hedgehog* and *decapentaplegic* expression by independent mechanisms. Development 129, 5697–5706.
Lee JA, Yerbury JJ, Farrawell N, Shearer RF, Constantinescu P, Hatters DM, Schroder WA, Suhrbier A, Wilson MR, Saunders DN, Ranson M (2015). SerpinB2 (PAI-2) modulates proteostasis via binding misfolded proteins and promotion of cytoprotective inclusion formation. PLoS One 10, e0130136.
Lek M, Karczewski KJ, Minikel EV, Samocha KE, Banks E, Fennell T, O'Donnell-Luria AH, Ware JS, Hill AJ, Cummings BB, *et al.* (2016). Analysis of protein-coding genetic variation in 60,706 humans. Nature 536, 285–291.
Liu Z, Xu J, He J, Zheng Y, Li H, Lu Y, Qian J, Lin P, Weber DM, Yang J, Yi Q (2014). A critical role of autocrine sonic hedgehog signaling in human $CD138^+$ myeloma cell survival and drug resistance. Blood 124, 2061–2071.
Lopes CA, Prosser SL, Romio L, Hirst RA, O'Callaghan C, Woolf AS, Fry AM (2011). Centriolar satellites are assembly points for proteins implicated in human ciliopathies, including oral-facial-digital syndrome 1. J Cell Sci 124, 600–612.
Mansfield E, Hersperger E, Biggs J, Shearn A (1994). Genetic and molecular analysis of hyperplastic discs, a gene whose product is required for regulation of cell proliferation in *Drosophilamelanogaster* imaginal discs and germ cells. Dev Biol 165, 507–526.
Matta-Camacho E, Kozlov G, Li FF, Gehring K (2010). Structural basis of substrate recognition and specificity in the N-end rule pathway. Nat Struct Mol Biol 17, 1182–1187.
May SR, Ashique AM, Karlen M, Wang B, Shen Y, Zarbalis K, Reiter J, Ericson J, Peterson AS (2005). Loss of the retrograde motor for IFT disrupts localization of Smo to cilia and prevents the expression of both activator and repressor functions of Gli. Dev Biol 287, 378–389.
McCloy RA, Rogers S, Caldon CE, Lorca T, Castro A, Burgess A (2014). Partial inhibition of Cdk1 in G 2 phase overrides the SAC and decouples mitotic events. Cell Cycle 13, 1400–1412.
McDermott KM, Liu BY, Tlsty TD, Pazour GJ (2010). Primary cilia regulate branching morphogenesis during mammary gland development. Curr Biol 20, 731–737.

Meissner B, Kridel R, Lim RS, Rogic S, Tse K, Scott DW, Moore R, Mungall AJ, Marra MA, Connors JM, *et al.* (2013). The E3 ubiquitin ligase UBR5 is recurrently mutated in mantle cell lymphoma. Blood 121, 3161–3164.
Michaud EJ, Yoder BK (2006). The primary cilium in cell signaling and cancer. Cancer Res 66, 6463–6467.
Mick DU, Rodrigues RB, Leib RD, Adams CM, Chien AS, Gygi SP, Nachury MV (2015). Proteomics of primary cilia by proximity labeling. Dev Cell 35, 497–512.
Moncrieff S, Moncan M, Scialpi F, Ditzel M (2015). Regulation of *hedgehog* ligand expression by the N-end rule ubiquitin-protein ligase hyperplastic discs and the *Drosophila* GSK3β homologue, Shaggy. PLoS One 10, e0136760.
Munoz-Escobar J, Matta-Camacho E, Kozlov G, Gehring K (2015). The MLLE domain of the ubiquitin ligase UBR5 binds to its catalytic domain to regulate substrate binding. J Biol Chem 290, 22841–22850.
Niehrs C, Pollet N (1999). Synexpression groups in eukaryotes. Nature 402, 483–487.
O'Brien PM, Davies MJ, Scurry JP, Smith AN, Barton CA, Henderson MJ, Saunders DN, Gloss BS, Patterson KI, Clancy JL, *et al.* (2008). The E3 ubiquitin ligase EDD is an adverse prognostic factor for serous epithelial ovarian cancer and modulates cisplatin resistance in vitro. Br J Cancer 98, 1085–1093.
Olson A, Sheth N, Lee JS, Hannon G, Sachidanandam R (2006). RNAi Codex: a portal/database for short-hairpin RNA (shRNA) gene-silencing constructs. Nucleic Acids Res 34, D153–D157.
Orlowski RZ, Stinchcombe TE, Mitchell BS, Shea TC, Baldwin AS, Stahl S, Adams J, Esseltine DL, Elliott PJ, Pien CS, *et al.* (2002). Phase I trial of the proteasome inhibitor PS-341 in patients with refractory hematologic malignancies. J Clin Oncol 20, 4420–4427.
O'Toole SA, Machalek DA, Shearer RF, Millar EK, Nair R, Schofield P, McLeod D, Cooper CL, McNeil CM, McFarland A, *et al.* (2011). Hedgehog overexpression is associated with stromal interactions and predicts for poor outcome in breast cancer. Cancer Res 71, 4002–4014.
Passmore LA, Barford D (2004). Getting into position: the catalytic mechanisms of protein ubiquitylation. Biochem J 379, 513–525.
Patzke S, Hauge H, Sioud M, Finne EF, Sivertsen EA, Delabie J, Stokke T, Aasheim HC (2005). Identification of a novel centrosome/microtubule-associated coiled-coil protein involved in cell-cycle progression and spindle organization. Oncogene 24, 1159–1173.
Patzke S, Redick S, Warsame A, Murga-Zamalloa CA, Khanna H, Doxsey S, Stokke T (2010). CSPP is a ciliary protein interacting with Nephrocystin 8 and required for cilia formation. Mol Biol Cell 21, 2555–2567.
Patzke S, Sternemalm J, Geimer S, Sun X, Aarnes EK, Stokke T, Pedersen LB. (2012). Role of CSPP-L in recruitment of ciliopathy proteins to centriolar satellites and the ciliary transition zone. Cilia 1 (Suppl 1), 36.
Patzke S, Stokke T, Aasheim HC (2006). CSPP and CSPP-L associate with centrosomes and microtubules and differently affect microtubule organization. J Cell Physiol 209, 199–210.
Pazour GJ, Agrin N, Leszyk J, Witman GB (2005). Proteomic analysis of a eukaryotic cilium. J Cell Biol 170, 103–113.
Reinhold WC, Sunshine M, Liu H, Varma S, Kohn KW, Morris J, Doroshow J, Pommier Y (2012). CellMiner: a web-based suite of genomic and pharmacologic tools to explore transcript and drug patterns in the NCI-60 cell line set. Cancer Res 72, 3499–3511.
Rieder CL, Jensen CG, Jensen LC (1979). The resorption of primary cilia during mitosis in a vertebrate (PtK1) cell line. J Ultrastruct Res 68, 173–185.
Rohatgi R, Milenkovic L, Scott MP (2007). Patched1 regulates hedgehog signaling at the primary cilium. Science 317, 372–376.
Roth KE, Rieder CL, Bowser SS (1988). Flexible-substratum technique for viewing cells from the side: some in vivo properties of primary (9+0) cilia in cultured kidney epithelia. J Cell Sci 89(Pt 4), 457–466.
Santiago-Sim T, Burrage LC, Ebstein F, Tokita MJ, Miller M, Bi W, Braxton AA, Rosenfeld JA, Shahrour M, Lehmann A, *et al.* (2017). Biallelic variants in OTUD6B cause an intellectual disability syndrome associated with seizures and dysmorphic features. Am J Hum Genet 100, 676–688.
Satir P, Christensen ST (2007). Overview of structure and function of mammalian cilia. Annu Rev Physiol 69, 377–400.
Saunders DN, Hird SL, Withington SL, Dunwoodie SL, Henderson MJ, Biben C, Sutherland RL, Ormandy CJ, Watts CK (2004). *Edd*, the murine hyperplastic disc gene, is essential for yolk sac vascularization and chorioallantoic fusion. Mol Cell Biol 24, 7225–7234.
Scheffner M, Nuber U, Huibregtse JM (1995). Protein ubiquitination involving an E1-E2-E3 enzyme ubiquitin thioester cascade. Nature 373, 81–83.
Schindelin J, Arganda-Carreras I, Frise E, Kaynig V, Longair M, Pietzsch T, Preibisch S, Rueden C, Saalfeld S, Schmid B, *et al.* (2012). Fiji: an open-source platform for biological-image analysis. Nat Methods 9, 676–682.
Serrao VH, Alessandro F, Caldas VE, Marcal RL, Pereira HD, Thiemann OH, Garratt RC (2011). Promiscuous interactions of human septins: the GTP binding domain of SEPT7 forms filaments within the crystal. FEBS Lett 585, 3868–3873.
Shaheen R, Shamseldin HE, Loucks CM, Seidahmed MZ, Ansari S, Ibrahim Khalil M, Al-Yacoub N, Davis EE, Mola NA, Szymanska K, *et al.* (2014). Mutations in CSPP1, encoding a core centrosomal protein, cause a range of ciliopathy phenotypes in humans. Am J Hum Genet 94, 73–79.
Shearer RF, Iconomou M, Watts CK, Saunders DN (2015). Functional roles of the E3 ubiquitin ligase UBR5 in cancer. Mol Cancer Res 13, 1523–1532.
Shearer RF, Saunders DN (2015). Experimental design for stable genetic manipulation in mammalian cell lines: lentivirus and alternatives. Genes Cells 20, 1–10.
Shearer RF, Saunders DN (2016). Regulation of primary cilia formation by the ubiquitin–proteasome system. Biochem Soc Trans 44, 1265–1271.
Shin KJ, Wall EA, Zavzavadjian JR, Santat LA, Liu J, Hwang JI, Rebres R, Roach T, Seaman W, Simon MI, Fraser ID (2006). A single lentiviral vector platform for microRNA-based conditional RNA interference and coordinated transgene expression. Proc Natl Acad Sci USA 103, 13759–13764.
Sternemalm J, Geimer S, Frikstad KA, Schink KO, Stokke T, Patzke S (2015). CSPP-L associates with the desmosome of polarized epithelial cells and is required for normal spheroid formation. PLoS One 10, e0134789.
Sternemalm J, Russnes HG, Zhao X, Risberg B, Nord S, Caldas C, Borresen-Dale AL, Stokke T, Patzke S (2014). Nuclear CSPP1 expression defined subtypes of basal-like breast cancer. Br J cancer 111, 326–338.
Stinson SF, Alley MC, Kopp WC, Fiebig HH, Mullendore LA, Pittman AF, Kenney S, Keller J, Boyd MR (1992). Morphological and immunocytochemical characteristics of human tumor cell lines for use in a disease-oriented anticancer drug screen. Anticancer Res 12, 1035–1053.
Stoilov P, Rafalska I, Stamm S (2002). YTH: a new domain in nuclear proteins. Trends Biochem Sci 27, 495–497.
Tasaki T, Zakrzewska A, Dudgeon DD, Jiang Y, Lazo JS, Kwon YT (2009). The substrate recognition domains of the N-end rule pathway. J Biol Chem 284, 1884–1895.
Tollenaere MA, Mailand N, Bekker-Jensen S (2015). Centriolar satellites: key mediators of centrosome functions. Cell Mol Life Sci 72, 11–23.
Tuz K, Bachmann-Gagescu R, O'Day DR, Hua K, Isabella CR, Phelps IG, Stolarski AE, O'Roak BJ, Dempsey JC, Lourenco C, *et al.* (2014). Mutations in CSPP1 cause primary cilia abnormalities and Joubert syndrome with or without Jeune asphyxiating thoracic dystrophy. Am J Hum Genet 94, 62–72.
van Noort V, Snel B, Huynen MA (2003). Predicting gene function by conserved co-expression. Trends Genet 19, 238–242.
Villumsen BH, Danielsen JR, Povlsen L, Sylvestersen KB, Merdes A, Beli P, Yang YG, Choudhary C, Nielsen ML, Mailand N, Bekker-Jensen S (2013). A new cellular stress response that triggers centriolar satellite reorganization and ciliogenesis. EMBO J 32, 3029–3040.
Wang L, Lee K, Malonis R, Sanchez I, Dynlacht BD (2016). Tethering of an E3 ligase by PCM1 regulates the abundance of centrosomal KIAA0586/Talpid3 and promotes ciliogenesis. Elife 5.
Wang G, Tang X, Chen Y, Cao J, Huang Q, Ling X, Ren W, Liu S, Wu Y, Ray L, Lin X (2014). Hyperplastic discs differentially regulates the transcriptional outputs of hedgehog signaling. Mech Dev 133, 117–125.
Wheway G, Schmidts M, Mans DA, Szymanska K, Nguyen TM, Racher H, Phelps IG, Toedt G, Kennedy J, Wunderlich KA, *et al.* (2015). An siRNA-based functional genomics screen for the identification of regulators of ciliogenesis and ciliopathy genes. Nat Cell Biol 17, 1074–1087.
Wu LF, Hughes TR, Davierwala AP, Robinson MD, Stoughton R, Altschuler SJ (2002). Large-scale prediction of *Saccharomyces cerevisiae* gene function using overlapping transcriptional clusters. Nat Genet 31, 255–265.
Zhang T, Cronshaw J, Kanu N, Snijders AP, Behrens A (2014). UBR5-mediated ubiquitination of ATMIN is required for ionizing radiation-induced ATM signaling and function. Proc Natl Acad Sci USA 111, 12091–12096.
Zhu L, Wang Z, Wang W, Wang C, Hua S, Su Z, Brako L, Garcia-Barrio M, Ye M, Wei X, *et al.* (2015a). Mitotic protein CSPP1 interacts with CENP-H protein to coordinate accurate chromosome oscillation in mitosis. J Biol Chem 290, 27053–27066.
Zhu Q, Wong AK, Krishnan A, Aure MR, Tadych A, Zhang R, Corney DC, Greene CS, Bongo LA, Kristensen VN, *et al.* (2015b). Targeted exploration and analysis of large cross-platform human transcriptomic compendia. Nat Methods 12, 211–214.